Fabrication of photocatalytically active vanadium oxide nanostructures via plasma route

Shin Kajita

*Institute of Materials and Systems for Sustainability, Nagoya University, Nagoya 464-8603, Japan**

Tomoko Yoshida

The Osaka City University Advanced Research Institute for Natural Science and Technology, Osaka 558-8585, Japan

Noriyasu Ohno, Yusuke Ichino

Graduate School of Engineering, Nagoya University, Nagoya 464-8603, Japan

Naoaki Yoshida

Research Institute for Applied Mechanics, Kyushu University, Kasuga, Fukuoka 816-8580, Japan

(Dated: March 20, 2018)

Abstract

Plasma irradiation was used to create nanostructured vanadium oxide with potential commercial and industrial applications. Morphology changes were induced at the nano- and micro-meter scale, accompanied by the growth of helium nanobubbles. Micrometer-sized pillars, cube-shaped nanostructures, and fuzzy fiberform nanostructures were grown on the surface; the necessary conditions in terms of the incident ion energy and the surface temperature for those morphology changes were revealed. Hydrogen production experiments using a photocatalytic reaction with aqueous methanol solution were conducted on the fabricated samples. Enhanced H_2 production was confirmed with the plasma irradiated nanostructured sample that had been oxidized in air atmosphere. Photocatalytically inactive vanadium oxide exhibited a high photocatalytic activity after nanostructurization of the surface by helium plasma irradiation.

PACS numbers:

*Electronic address: kajita.shin@nagoya-u.jp

I. INTRODUCTION

Vanadium (V) oxides can be used in various applications including energy storage [1], batteries [2], sensors [3], nanobeams [4], chemical catalysts [5], and photocatalysts [6–8]. Because nanostructures and micro-structures can improve the performance in devices by increasing its surface area, various methods have been utilized to fabricate mesoporous V oxides such as the sol-gel process [9], the hydrothermal process [10], the polyol process [11], and ion beam sputtering [12]. As a photocatalyst, V oxides is a candidate material for photo-assisted water-splitting devices, particularly because its band gap is lower than the 3.0-3.2 eV range of titanium dioxide (TiO_2) [7]. However, only a limited number of studies have been reported on the photocatalytic activity of V oxides for H_2 production [7, 8, 10].

In the mid-2000s, it was discovered that fiberform nanostructures called fuzz was grown on tungsten surface by helium (He) plasma irradiation [13]. He atoms implanted on the surface form clusters and He bubbles near the surface while diffusing in the W matrix [14]. Sub-micrometer sized protrusions and pinholes occurred in conjunction with the He bubble growth [15]. Those initial morphology changes are thought to develop into fiberform nanostructures. Similar fuzzy nanostructure growth has been identified on other metals including molybdenum, nickel, titanium, iron, rhenium, and tantalum [16–21], indicating that significant morphology changes accompanied by the He bubble growth are common to many metals. As the plasma irradiation's bottom up approach only requires a one-step dry process [22], materials fabricated using this process are anticipated to be useful for industrial application. Oxidized helium irradiated tungsten and titanium have been explored as potential photocatalytic materials. Partially oxidized fuzzy tungsten had a visible light response to decompose methylene blue [23] and enhanced performance to split water [24]. On oxidized nanostructured Ti, it was also identified that the efficiency of H_2 production from aqueous methanol solution was enhanced by the formation of nanostructures [25]. He plasma irradiation of V was recently reported to create whisker like structures on the metal surface [26]; however, fuzzy nanostructure formation on V has yet to be disclosed. Morphology changes and necessary conditions for fuzz formation strongly depend on materials. The shear modulus was likely to be an important parameter whether fuzz can be formed by He plasma irradiation [27]. The shear modulus of vanadium in room temperature is 47 GPa, which is much lower than that of molybdenum and tungsten; V is categorized in the metal

where fuzzy structures are not easily formed. Thus, it is of importance to conduct systematic He plasma irradiations to V sample and identify the relationship between the irradiation condition and morphology changes.

In this study, we show that He plasma irradiation causes various morphology changes, including fiberform nanostructures, to occur on the V surface. Performing systematic experiments varying the surface temperature and the incident ion energy of the plasma irradiations, we identified the necessary irradiation conditions to form fuzzy fiberform V nanostructures. The resulting samples were characterized by scanning electron microscope (SEM), transmission electron microscope (TEM), thermal desorption spectroscopy (TDS), and X-ray photoelectron spectroscopy (XPS). Optical reflectance measurements were also taken. Using these fabricated samples, we conducted photocatalytic experiments to evaluate H_2 production from a methanol solution. These experiments demonstrated that nanostructurization by He irradiation activated the photocatalytic reactivity of V_2O_5 to produce H_2.

II. METHODS

A. Helium plasma irradiation

He plasma irradiation was conducted using the linear plasma device NAGDIS-II [18]. In the NAGDIS-II device, as described in [28], high density plasma up to 10^{20} m^{-3} can be produced in a steady state. The plasma is produced between a 108 mm diameter LaB_6 cathode, which is heated by a carbon heater with a typical heating power of 3 kW, and a hollow anode made of copper. A cusp magnetic field is employed to confine the plasma from the source region. Typically, the discharge voltage for He plasmas is $\sim$100 V. The length of the plasma was approximately 2.5 m, and the irradiation region was $\sim$1.5 m away from the plasma source region. Figure 1(a) shows a schematic of the experimental setup for the He plasma irradiation. A V plate with a thickness of 0.1 mm was used for the irradiation experiments. Before the plasma irradiation, the roughness R_a of the sample measured by a laser microscope (VK-9510, Keyence) was 0.44 μm. As shown in the later section, the top surface layer ($\ll$1 μm) was oxidized and composed of intermixed V(III) and V(IV) oxides and a V(V) oxide layer. The major grains identified before the plasma exposure were V (200) and (211).

The sample was installed on a water cooling stage to control the irradiation temperature, particularly when the surface temperature was <1000 K. The incident ion energy was controlled by biasing the sample negatively. The surface temperature was measured with a radiation pyrometer, and the ion flux was measured with an electrostatic probe located ∼30 cm upstream of the region where the sample was installed. The sample was placed in the center of the plasma column, and the sample normal was rotated ∼45 degree from the magnetic field line to measure the temperature from the viewing port. Since the ions were accelerated in the electric sheath formed in front of the sample, the ions were impinged on the surface almost from the normal direction. The He flux can be controlled in the range of 0.1-10$\times 10^{22}$ $m^{-2}s^{-1}$ by changing the magnetic field strength and the discharge current. In this study, the discharge current and the He ion flux were in the ranges of 10-25 A and 0.9-2.6$\times 10^{22}$ $m^{-2}s^{-1}$, respectively. The He gas pressure was ∼11 mTorr. The magnetic field strength in the source region was 0.1 T, but it was decreased to one fourth of the value in the downstream region to control the flux to the sample. The sample was exposed to the plasma for 1 hour.

B. Photocatalytic experiments

Figure 1(b) shows a schematic of the experimental setup for the photocatalytic H_2 production experiment. The amount of the H_2 produced from a 20 vol% aqueous methanol solution was measured using a gas chromatograph (Shimadzu, GC-8A). Methanol is frequently used as a sacrificial reagent to enhance the H_2 production from the reduction of H_2O, and the amount of 20 vol% was a typical value used for H_2 production experiments from a methanol solution [29]. A xenon lamp was used for the light source, and a cold ultra violet (UV) mirror and a short-pass optical filter of 430 nm was utilized to select for UV light; the UV power measured 2.0 mW/cm^2. The sample material used for the photocatalytic experiments had a surface area of 10×10 mm^2 and was 0.1 mm thick. The sample and 10 ml of aqueous methanol solution were installed in a cylindrical-shaped quartz reactor whose diameter and height are ∼40 and 200 mm, respectively. Before irradiation, the air inside the reactor was evacuated using a rotary pump, and the pressure inside the reactor was ∼30-50 Torr during the UV irradiation.

III. MORPHOLOGY CHANGES

Figure 2(a-c) shows the SEM micrographs of the He plasma irradiated V samples, and blisters, protrusion, and pinholes were formed on the surfaces. Figure 2(a,b) are the SEM micrographs of the same sample at different magnifications. The surface temperature, the incident ion energy, and the He fluence in Figs. 2(a,b) and 2(c) were 760 K, 115 eV, and 1.6×10^{25} m^{-2} and 730 K, 115 eV, and 1.3×10^{26} m^{-2}, respectively. Because the temperature was determined by the heat flux from the plasma and the heat resistance between the cooling stage and the sample, it was not easy to control them separately. The major difference for these two samples was originated from the difference in the fluence, and difference in the temperature by 30 K was not significant, as shown later. Many white spots were observed on the surface of both the samples. The sizes of the spots are less than 200-300 nm in Fig. 2(a,b), and it increased significantly when the He fluence is higher in Fig. 2(c), though the incident ion energy and the temperature were similar. The sizes of the spot were more uniform in Fig. 2(c) than those in Fig. 2(a,b). The subtle difference in the temperature did not cause this difference. Because similar uniform spot size distribution was identified even at the surface temperature of 890 K and the fluence of 6.1×10^{25} m^{-2}, it was likely that the uniform size distribution appeared when the fluence was higher than $\sim5\times10^{25}$ m^{-2}.

Although those structures have not been identified on tungsten samples exposed to He plasmas, they were similar to the voids and nano-pillars formed on aluminum, copper, and titanium surfaces exposed to He plasmas [30]. It was discussed that He ions induced void growth and physical sputtering played a key role for the morphology changes. Because the sputtering threshold energy of V by He ion bombardment is $\sim$30 eV [31], it is noted that considerable sputtering occurs in the present study. Combination of physical sputtering, deposition, and He bubble growth are likely to be deeply related with the morphology changes. As shown in the inset of Fig. 2(b), in addition to white spots, black dots (pinholes) were identified on the surface. The pinholes have been frequently observed on He irradiated surfaces and were caused by He bubbles formed beneath the surface [32]; the pinholes indicated the formation of He bubbles, which will be discussed later with TEM observations.

Figure 3(a-c) shows SEM micrographs of He plasma irradiated V surfaces when the surface temperature was higher than 1000 K during the irradiation. The temperature, the incident ion energy and the He fluence were, respectively, (a) 1130 K, 75 eV, and 4.3×10^{25}

m^{-2}; (b) 1040 K, 115 eV, and 4.8×10^{25} m^{-2}; and (c) 1110 K, 115 eV, and 9.4×10^{25} m^{-2}. It is seen that fuzzy structures were observed on the surfaces when the incident ion energy was 115 eV. The results suggested that there existed an energy threshold around 100 eV to form fuzzy structures on V surface. In addition, cube shaped structures are found in Fig. 3(b,c) when the fuzzy structures were grown on the surface. Tripathi *et al.* irradiated V samples with He ions at the incident ion energy of 100 eV in the surface temperature range of 823-1173 K [26]. In Ref. [26], sub-micrometer sized cube shaped surface pores were homogenously formed on V samples after the He plasma irradiation, and the size of these pores increased with the surface temperature. Moreover, whiskers were observed when the surface temperature was around 1000 K, which is consistent with the temperature where fuzz appeared in this study. Since the He fluence and flux in this study was one order of magnitude higher than those in [26], the whiskers grew into fuzzy structures.

Figure 4(a-c) shows TEM micrographs of a V sample exposed to He plasma. Techniques such as a focused ion beam or electric polishing are usually used to prepare TEM sample. However, those methods might damage the fuzzy structures or would require coating on the surface. In this study, we used a semi-circular 3 mm in diameter sample, which can be installed to TEM sample stage directly, for this irradiation in particular. The incident ion energy was 110 eV, the surface temperature was 1090 K, and the ion fluence was 8.9×10^{25} m^{-2}. Fine fibers that were less than 50 nm in diameter can be seen entangled together: the feature is quite similar to W fuzz [15]. As shown in Fig. 4(b,c), many He bubbles are visible inside the structure. The He bubbles were not ideal spherical or hexagonal shapes. The shape of He bubbles would be spherical when the He gas pressure inside the bubble was balanced with the surface tension [33]. Irregular shapes indicated that the inner pressure was less than the equilibrium pressure, probably because of an active supply of thermal vacancies to He bubbles [34]. The size of the He bubbles are mostly less than 10 nm in diameter; a few bubbles are larger than 20 nm. On the surface, a thin ($\sim$2 nm) layer can be identified that presumably corresponds to the oxidized layer. When the sample was oxidized in the air atmosphere, the surface was covered by $\sim$2 nm thick oxidized layer. The layer would be much thicker if the sample had been oxidized while heating, as will be done later.

To understand the migration of He inside the V sample, it is helpful to analyze the gas desorption properties. Figure 5 shows the TDS spectrum from a He irradiated V sample at 843 K. The temperature was increased from room temperature at a rate of $\sim$1.1 K/s. Two

large desorption peaks were identified at 1000 and 1250 K. Similar to other metals [20, 35], the gas desorption around the low temperature peak indicates the onset of the significant He migration that would be required for the growth of He bubbles and the formation of fuzzy structures. On the other hand, if too much He desorption occurs, these fine structures would be reintegrated to the surface. Likely, it would be difficult to form these structures when the temperature was sufficiently higher than 1250 K, although we did not conduct experiments at that temperature range.

Figure 6 summarizes the relationship between the morphology changes on the V surfaces and the corresponding irradiation conditions, i.e., the incident ion energy and the surface temperature (these are the key parameters for the morphology changes for tungsten [16]). The He fluence plotted in Fig. 6 was in the range of 5×10^{24} - 1.3×10^{26} m^{-2}. When the surface temperature was less than 900 K and the incident ion energy was lower than 100 eV, no significant morphology changes were observed. The surface was flat even after the He plasma irradiation. When either the surface temperature or the incident ion energy increased, the surface became rough with nanopillar or micropillar-like structures and pinholes. When the surface temperature was higher than 1000 K and the incident ion energy was higher than 100 eV, fuzzy structures were observed on the surface. As discussed with TDS spectrum, this temperature dependence can be explained by the He migration and the formation of He clusters. A recent object kinetic Monte Carlo simulation explained the temperature dependence of W fuzz growth as being based on the trapping and de-trapping of He in He-vacancy clusters [36]. To our knowledge, the incident ion energy dependence has yet to be well understood. Although He atoms can be implanted on W when the incident ion energy is higher than $\sim$5 eV [37], the threshold energy for fuzz growth does not agree with the energy. Subtle difference in the penetration depth may be related to the consequent He migration [38], but no quantitative analysis has been provided. In the case of tungsten, a minimum threshold energy for fuzz growth is recognized to be around 20-30 eV. At the moment, we cannot explain the mechanism that causes V nanostructure growth to occur at a higher threshold energy than that of W.

When fine structures were formed on the V surface, the surface turned visually black. The optical reflectance (including specular and diffuse reflectance) was measured by a spectrophotometer (UV-2600, Shimadzu, Co.), which equips a small integrating sphere. Figure 7 shows the wavelength dependence of the optical reflectance of a pristine V sample and

of the V samples exposed to the He plasmas at 990, 1120, and 1190 K. The incident ion energy was 115 eV for all three samples. On the sample exposed at 990 K, micro-pillars were observed, while the samples exposed at 1120 and 1190 K had fuzzy structures. On the pristine V sample, the optical reflectance was higher than 50% at the wavelength of >350 nm. The optical reflectance decreased when the wavelength was less than 350 nm and was 30% at 250 nm. The optical reflectance significantly decreased in a wide wavelength from UV to visible range on all three samples exposed to the He plasmas. At a wavelength range shorter than 500 nm, the optical reflectance was less than 5% for all the three samples. At longer wavelengths, the reduction ratio was higher for higher irradiation temperature. For example, the reflectance at 800 nm decreased from 17% at 990 K to 6% at 1190 K. When the irradiation temperature was 990 K, since the scale length of roughness should be smaller than that at 1190 K, the reflectance is lower for a shorter wavelength range (<500 nm) and higher for a longer wavelength range (>500 nm) compared to that of the 1190 K irradiation sample.

Blackening has also been observed on fuzzy W [39], presumably because the material properties were significantly changed. In metals, the free electron density is an important parameter to determine the plasma frequency [40]. Since the density decreased by an order of magnitude due to the fuzz formation [41], it is likely that the reflectance decreased due to the decrease in the plasma frequency. Although the decrease in the optical reflectance does not necessarily correspond to electron excitation on the oxidized V surface layer, there is a possibility that electron excitation may be higher after nanostructure formation.

IV. PHOTOCATALYTIC EXPERIMENTS

As summarized in Table I, we used four samples (V1-V4) for H_2 production experiments: a pristine V sample without any treatment (V1), an oxidized V sample (V2), a nanostructured V sample (V3), and an oxidized nanostructured V sample (V4). For V3 and V4, during plasma irradiation, the surface temperature was ∼1070 K and the incident ion energy was 115 eV. For V2 and V4 samples, the oxidization was conducted using a furnace at 773 K for 0.5 hours.

Figure 8 shows the XPS V2p spectra of V1-V4 after calibrating the energy using the O 1s peak at 530.0 eV. A mixture of five different oxidation states can be found in vanadium

oxides, and it is not simple to define the phases from XPS analysis. The five oxidation states have V2p peaks in the energy range of 512.35 (V^{0+}) to 517.2 (V^{5+}), as indicated by dotted lines in Fig. 8 [42]. All the samples have a peak at 517.2 eV, corresponding to V^{+5}, suggesting the existence of V_2O_5. However, the fact that the spectra was broader than pure V_2O_5 spectrum indicated the existence of several intermixed phases from V^{5+} to V^{3+} [43]. Previously, even on VO_2 (V^{4+}) powder pellet, a V^{5+} peak was identified due to an over oxidized layer on the surface [42]. Thus, the broadened spectrum with its peak at 517.2 eV indicated that intermixed V(III) and V(IV) oxides were covered by a V(V) oxide layer. The difference between the samples was not clearly identified from the XPS spectrum, which has a sensitivity in the range of ∼10 nm. The TEM observation in Fig. 4(c) was conducted four days after the He plasma irradiation, and the thickness of the oxidized layer was 2-3 nm. On the other hand, the XPS analysis and photocatalysis experiments were conducted about eight months after the irradiation; the thickness of the oxidized layer could be much greater than that observed in Fig. 4(c).

Figure 9 shows the X-ray diffraction (XRD) pattern of the four vanadium samples. Copper K-α was used for the radiation source, and the XRD had a sensitivity up to the depth of ∼1 μm. Two vanadium peaks can be identified at 60.9 (200) and 76.7 (211) degrees [44]. The V peak intensity decreased after plasma irradiation. This could be caused by a decrease in the size of the crystal grains due to the nanostructurization. Also, the spectrum became sharper on V3 compared to V1, indicating that the bulk crystal structure improved during plasma irradiation by an annealing effect. The ratio of the intensities at 60.9 and 76.7 degrees was altered from V1 to V4; the 76.7 degree peak almost disappeared on V4 sample. This suggests that the crystal structure was altered during these processes, partially because of recrystallization as it was observed at 873 K [45]. A peak at 27.7 degree, which corresponds to the VO_2 peak [46], was identified on the samples oxidized at 773 K (V2 and V4). It is noted that a peak corresponding to V_2O_5 (possibly in the range of 20.3-21.7 degrees) is not identified on any of the samples. After the plasma irradiation, small peaks appeared at ∼42 and 65 degrees on V3. The peak at ∼42 degree is likely to correspond to V (110). Because only V (200) and (211) peaks were observed before the plasma irradiation, the results suggested that the plasma irradiation slightly changed the crystal orientation. The peak at ∼65 degree could correspond to VO_2 (301) or VO (220) [47]. However, since the peak at ∼65 degree still remained even on V4 sample, it is unlikely that difference appeared

on V3 increased the photocatalytic reactivity shown later. From the XRD analysis, it was found that oxidization at 773 K formed a VO_2 layer on the metallic bulk V; the thickness could be less than 1 μm, but it was likely much thicker than 100 nm.

Figure 10(a) shows the time course of the H_2 produced from the 20 vol.% aqueous methanol solution by UV light irradiation. The H_2 increased with time in all cases including the blank case (control experiment), where no photocatalyst was introduced. Except for the V fuzz sample, the hydrogen produced was less than that of the blank sample, indicating that no clear photocatalytic reaction occurred on the pristine and oxidized samples, i.e., on V1, V2, and V4.

These results were similar to W case, where methylene blue decomposition by visible light irradiation was occurred only on a fuzzy W sample oxidized in the air atmosphere [23]. Even though V_2O_5 is originally inactive. it is known to become photocatalytically active when it is highly dispersed on silica [48]. Nanostructurization can alter the band and potential structures, and, consequently, change the photocatalytic reactivity. Similar to the highly dispersed cases, the photocatalytic activity was exhibited on the nanostructured sample. The reason photocatalytic activity was exhibited only on V3 sample, where nanostructured V was oxidized in the air atmosphere, could be attributed to the fact that the surface was covered with nanometer sized V oxides, similar to the W case. On fuzzy WO_3, the interface between WO_3/W was crucial for methylene blue decomposition by photocatalysis. The initial photo-excitations due to the surface plasmon resonance followed by electron injections into the conduction band of the nano-sized WO_3 moiety at the WO_3/W interface likely caused a chemical reaction to occur on the sample surface [49]. Similarly, there was a possibility that photo-excitation and electron injection have occurred in the interface between V and V oxides near the surface and contributed to proceed the reaction. This interface did not exist on V2 and V4 samples, because V had changed to VO_2, and the nanostructures did not exist on V1.

Figure 10(b) summarizes the amount of hydrogen produced by 2 hours of UV light irradiation. The hydrogen was produced at $\sim$2.5 μmol for two hours from the blank case. On the fuzzy V sample without oxidization (V3), the hydrogen production was significantly higher than that of the background level. It was confirmed that hydrogen production occurred by photocatalytic reaction. In Fig. 10(b), the same experiments were conducted three times for V3 using the same sample. The hydrogen production efficiency was sufficiently higher than

that of the blank case even on the third iteration, confirming the repeatability of the V3 sample's photocatalytic reactivity. The amount of hydrogen produced for two hours was 3.9 μmol from the nanostructured V sample without additional oxidization. Subtracting the background hydrogen production, the effective hydrogen production rate was 0.7 μmol/h from the fuzzy V sample. For the unit area, this corresponds to 7 mmol/m^2/h at 2.0 mW/cm^2 UV irradiation. Photocatalytic hydrogen production experiments from aqueous methanol solutions have also been conducted using microstructured TiO_2 formed using He plasmas [25]. The amount of hydrogen produced was $\sim$0.4 μmol/h, which was 60% higher than the TiO_2 sample without He plasma irradiation. Although the aqueous solution was different and the UV power was likely to be slightly altered, the hydrogen production capability of the fuzzy V sample was similar to or greater than that of the TiO_2 sample fabricated using He plasmas. This value was lower in efficiency by approximately one order of magnitude compared to the previously reported 800 mmol/m^2/h at 27 mW/cm^2 UV irradiation using nanostructured VO_2 photocatalysts [7]. Degradation of crystallinity by the formation of He bubbles/clusters and the difference in the height of the nanostructured layer are potential reasons to cause the difference in the efficiency. We expect to achieve improvements by using samples exposed to the plasma under different conditions and different oxidation states. In this study, the photocatalytic experiments were conducted using samples exposed to the air for long time ($\sim$8 months). Thus, it is important to investigate the aging behavior and the optimum exposure time to the air for considering practical applications.

V. CONCLUSIONS

In this study, vanadium plates were subjected to helium plasma irradiation under varying irradiation conditions of surface temperature and incident ion energy. In addition to nano/micro-pillars, fiberform nanostructures were formed when the surface temperature was higher than $\sim$1000 K and the incident ion energy was higher than 110 eV. When nanostructures were formed on the surface, the optical reflectance decreased to less than 10% from UV to visible wavelengths. Transmission electron microscope (TEM) observation of the fabricated V nanostructures revealed that He bubbles existed inside the structure and that the nanostructures were covered with a 2-3 nm thick oxide layer. Although fuzzy nanostructures have been formed on other metals such as tungsten and molybdenum, this is the first time

that fiberform structures have been identified on a vanadium surface. These results indicate that the nanostructure growth can occur on most metals, except for those with a low shear modulus [20].

Photocatalytic activity was investigated using hydrogen production from a 20 vol.% aqueous methanol solution under UV light irradiation. Four samples were tested: a pristine V sample, an oxidized V sample at 773 K, a nanostructured V sample, and an oxidized nanostructured V sample. XPS analysis confirmed that intermixed V(III) and V(IV) oxides were covered by a V(V) oxide layer on all the samples. Only the nanostructured V sample oxidized in the air atmosphere had the capability to produce hydrogen. The other three samples were photocatalytically inactive. This suggests that nanostructurization by plasma irradiation enhances the photocatalytic activity in a similar fashion to highly dispersed photocatalysts. Because vanadium oxides are used in various fields of research, it is of interest to investigate the applicability of these findings to other usages, including batteries, sensors, and photocatalysts.

Acknowledgment

Authors thank Mr. Nagata from NIFS for the support of TEM observation and Prof. H. Yoshida from Kyoto University for useful comments. This work was supported in part by a Grant-in-Aid for Scientific Research (B) 15H04229, a Grant-in-Aid for Exploratory Research 16K13917 from the Japan Society for the Promotion of Science (JSPS), and JSPS Bilateral Joint Research Project.

[1] Y. Wu, G. Gao, G. Wu, Self-assembled three-dimensional hierarchical porous V2O5/graphene hybrid aerogels for supercapacitors with high energy density and long cycle life, J. Mater. Chem. A, 3 (2015) 1828–1832.

[2] Y. Yue, H. Liang, Micro- and nano-structured vanadium pentoxide (V2O5) for electrodes of lithium-ion batteries, Advanced Energy Materials, 7 (2017) 1602545.

[3] J. Liu, X. Wang, Q. Peng, Y. Li, Vanadium pentoxide nanobelts: Highly selective and stable ethanol sensor materials, Advanced Materials, 17 (2005) 764–767.

[4] M. A. Huber, M. Plankl, M. Eisele, R. E. Marvel, F. Sandner, T. Korn, C. Schuller, R. F. Haglund, R. Huber, T. L. Cocker, Ultrafast mid-infrared nanoscopy of strained vanadium dioxide nanobeams, Nano Letters, 16 (2016) 1421–1427.

[5] M. Sutradhar, L. M. Martins, M. F. C. G. da Silva, A. J. Pombeiro, Vanadium complexes: Recent progress in oxidation catalysis, Coordination Chemistry Reviews, 301 (2015) 200 – 239.

[6] M. Anpo, M. Sunamoto, M. Che, Preparation of highly dispersed anchored vanadium oxides by photochemical vapor deposition method and their photocatalytic activity for isomerization of trans-2-butene, The Journal of Physical Chemistry, 93 (1989) 1187–1189.

[7] Y. Wang, Z. Zhang, Y. Zhu, Z. Li, R. Vajtai, L. Ci, P. M. Ajayan, Nanostructured VO2 photocatalysts for hydrogen production, ACS Nano, 2 (2008) 1492–1496.

[8] T. Puangpetch, S. Chavadej, T. Sreethawong, Mesoporous-assembled V2O5 nanosheet synthesized via a surfactant-modified sol-gel technique and its photocatalytic H2 production activity under visible light irradiation, Powder Technology, 208 (2011) 37 – 41.

[9] D. V. Raj, N. Ponpandian, D. Mangalaraj, C. Viswanathan, Effect of annealing and electrochemical properties of sol-gel dip coated nanocrystalline V2O5 thin films, Materials Science in Semiconductor Processing, 16 (2013) 256 – 262.

[10] T. F.-R. Shen, M.-H. Lai, T. C.-K. Yang, I.-P. Fu, N.-Y. Liang, W.-T. Chen, Photocatalytic production of hydrogen by vanadium oxides under visible light irradiation, Journal of the Taiwan Institute of Chemical Engineers, 43 (2012) 95 – 101.

[11] I. Mjejri, L. Manceriu, M. Gaudon, A. Rougier, F. Sediri, Nano-vanadium pentoxide films for electrochromic displays, Solid State Ionics, 292 (2016) 8 – 14.

[12] D. Zintu, G. Tosone, A. Mercuri, Dual ion beam sputtering vanadium dioxide microbolometers by surface micromachining, Infrared Physics & Technology, 43 (2002) 245 – 250.

[13] S. Takamura, N. Ohno, D. Nishijima, S. Kajita, Formation of nanostructured tungsten with arborescent shape due to helium plasma irradiation, Plasma Fusion Res., 1 (2006) 051.

[14] S. Krasheninnikov, T. Faney, B. Wirth, On helium cluster dynamics in tungsten plasma facing components of fusion devices, Nuclear Fusion, 54 (2014) 073019.

[15] S. Kajita, N. Yoshida, N. Ohno, Y. Tsuji, Growth of multifractal tungsten nanostructure by he bubble induced directional swelling, New Journal of Physics, 17 (2015) 043038.

[16] S. Kajita, W. Sakaguchi, N. Ohno, N. Yoshida, T. Saeki, Formation process of tungsten nanostructure by the exposure to helium plasma under fusion relevant plasma conditions, Nuclear Fusion, 49 (2009) 095005.

[17] G. De Temmerman, K. Bystrov, J. J. Zielinski, M. Balden, G. Matern, C. Arnas, L. Marot, Nanostructuring of molybdenum and tungsten surfaces by low-energy helium ions, Journal of Vacuum Science & Technology A, 30 (2012) 041306.

[18] S. Kajita, T. Yoshida, D. Kitaoka, R. Etoh, M. Yajima, N. Ohno, H. Yoshida, N. Yoshida, Y. Terao, Helium plasma implantation on metals: Nanostructure formation and visible-light photocatalytic response, Journal of Applied Physics, 113 (2013) 134301.

[19] S. Takamura, Y. Uesugi, Experimental identification for physical mechanism of fiber-form nanostructure growth on metal surfaces with helium plasma irradiation, Applied Surface Science, 356 (2015) 888 – 897.

[20] S. Kajita, T. Ishida, N. Ohno, D. Hwangbo, T. Yoshida, Fuzzy nanostructure growth on Ta/Fe by he plasma irradiation, Sci. Rep., 6 (2016) 30380.

[21] K. Omori, A. M. Ito, K. Shiga, N. Yamashita, K. Ibano, H. T. Lee, Y. Ueda, Comparison between helium plasma induced surface structures in group 5 (Nb, Ta) and group 6 elements (Mo, W), Journal of Applied Physics, 121 (2017) 155301.

[22] S. Iyyakkunnel, L. Marot, B. Eren, R. Steiner, L. M. D. Mathys, M. D. P. Chapon, E. Meyer, Morphological changes of tungsten surfaces by low-flux helium plasma treatment and helium incorporation via magnetron sputtering, ACS Applied Materials & Interfaces, 6 (2014) 11609 – 11616.

[23] K. Komori, T. Yoshida, T. Nomoto, M. Yamamoto, C. Tsukada, S. Yagi, M. Yajima, S. Kajita, N. Ohno, Sulfur k-edge XANES for methylene blue in photocatalytic reaction over WO3

nanomaterials, Nuclear Instruments and Methods in Physics Research Section B: Beam Interactions with Materials and Atoms, 365, Part A (2015) 35 – 38.

[24] M. de Respinis, G. De Temmerman, I. Tanyeli, M. C. van de Sanden, R. P. Doerner, M. J. Baldwin, R. van de Krol, Efficient plasma route to nanostructure materials: Case study on the use of m-WO3 for solar water splitting, ACS Applied Materials & Interfaces, 5 (2013) 7621–7625.

[25] S. Kajita, T. Yoshida, N. Ohno, T. Ishida, D. Kitaoka, Enhancement of photocatalytic activity of TiO2 by plasma irradiation, Japanese Journal of Applied Physics, 55 (2016) 106202.

[26] J. Tripathi, T. Novakowski, A. Hassanein, Tuning surface porosity on vanadium surface by low energy He+ ion irradiation, Applied Surface Science, 378 (2016) 63 – 72.

[27] S. Kajita, T. Nojima, Y. Tomita, N. Ohno, H. Tanaka, N. Yoshida, M. Yajima, T. Akiyama, M. Tokitani, T. Yagi, Fuzzy nanostructure growth on precious metals by he plasma irradiation, Surface and Coatings Technology, 340 (2018) 86 – 92.

[28] N. Ohno, D. Nishijima, S. Takamura, Y. Uesugi, M. Motoyama, N. Hattori, H. Arakawa, N. Ezumi, S. Krasheninnikov, A. Pigarov, U. Wenzel, Static and dynamic behaviour of plasma detachment in the divertor simulator experiment NAGDIS-II, Nuclear Fusion, 41 (2001) 1055.

[29] F. Guzman, S. S. C. Chuang, C. Yang, Role of methanol sacrificing reagent in the photocatalytic evolution of hydrogen, Industrial & Engineering Chemistry Research, 52 (2013) 61–65.

[30] I. Tanyeli, L. Marot, D. Mathys, M. C. M. van de Sanden, G. D. Temmerman, Surface modifications induced by high fluxes of low energy helium ions, Scientific Reports, 5 (2015) 9779.

[31] N. Matsunami, Y. Yamamura, Y. Itikawa, N. Itoh, Y. Kazumata, S. Miyagawa, K. Morita, R. Shimizu, H. Tawara, Energy dependence of the ion-induced sputtering yields of monatomic solids, Atomic Data and Nuclear Data Tables, 31 (1984) 1 – 80.

[32] S. Kajita, A. M. Ito, N. Ohno, Fractality and growth of He bubbles in metals, Physics Letters A, 381 (2017) 2355 – 2362.

[33] S. Donnelly, The density and pressure of helium in bubbles in implanted metals: a critical review, Radiation Effects, 90 (1985) 1–47.

[34] S. Kajita, N. Yoshida, R. Yoshihara, N. Ohno, M. Yamagiwa, Tem observation of the growth process of helium nanobubbles on tungsten: Nanostructure formation mechanism, J. Nucl. Mater, 418 (2011) 152 – 158.

[35] M. Yajima, N. Yoshida, S. Kajita, M. Tokitani, T. Baba, N. Ohno, In situ observation of structural change of nanostructured tungsten during annealing, Journal of Nuclear Materials, 449 (2014) 9 – 14.

[36] G. Valles, I. Martin-Bragado, K. Nordlund, A. Lasa, C. Bjorkas, E. Safi, J. Perlado, A. Rivera, Temperature dependence of underdense nanostructure formation in tungsten under helium irradiation, Journal of Nuclear Materials, 490 (2017) 108 – 114.

[37] D. Nishijima, M. Ye, N. Ohno, S. Takamura, Formation mechanism of bubbles and holes on tungsten surface with low-energy and high-flux helium plasma irradiation in nagdis-ii, J. Nucl. Mater, 329-333 (2004) 1029–1033.

[38] M. Yajima, M. Yamagiwa, S. Kajita, N. Ohno, M. Tokitani, A. Takayama, S. Saito, A. M. Ito, H. Nakamura, N. Yoshida, Comparison of damages on tungsten surface exposed to noble gas plasmas, Plasma Science and Technology, 15 (2013) 282.

[39] S. Kajita, T. Saeki, N. Yoshida, N. Ohno, A. Iwamae, Nanostructured black metal: Novel fabrication method by use of self-growing helium bubbles, Applied Physics Express, 3 (2010) 085204.

[40] M. Fox, Optical properties of solids, Oxford Unv. Press, Oxford, 2002.

[41] D. Nishijima, M. Baldwin, R. Doerner, J. Yu, Sputtering properties of tungsten 'fuzzy' surfaces, J. Nucl. Mater, 415 (2011) S96–S99.

[42] G. Silversmit, D. Depla, H. Poelman, G. B. Marin, R. D. Gryse, Determination of the V2p XPS binding energies for different vanadium oxidation states (V5+ to V0+), Journal of Electron Spectroscopy and Related Phenomena, 135 (2004) 167 – 175.

[43] M. Demeter, M. Neumann, W. Reichelt, Mixed-valence vanadium oxides studied by XPS, Surface Science, 454-456 (2000) 41 – 44.

[44] Y. Xu, M. Yamazaki, P. Villars, Inorganic materials database for exploring the nature of material, Japanese Journal of Applied Physics, 50 (2011) 11RH02.

[45] T. Nagasaka, H. Takahashi, T. Muroga, T. Tanabe, H. Matsui, Recovery and recrystallization behavior of vanadium at various controlled nitrogen and oxygen levels, Journal of Nuclear Materials, 283-287 (2000) 816 – 821.

[46] Y. Li, S. Ji, Y. Gao, H. Luo, M. Kanehira, Core-shell VO2@ TiO2 nanorods that combine thermochromic and photocatalytic properties for application as energy-saving smart coatings, Scientific reports, 3 (2013) 1370.

[47] R. W. G. Wyckoff, Absorption correction in precision determination of lattice parameters, Crystal structures, 1 (1963) 85,239.

[48] S. Yoshida, Y. Magatani, S. Noda, T. Funabiki, Partial oxidation of propene over uv-irradiated vanadium oxide supported on silica, Chemical Communications (1981) 601–602.

[49] K. Komori, T. Yoshida, S. Yagi, H. Yoshida, M. Yajima, S. Kajita, N. Ohno, Application of nanostructured tungsten fabricated by helium plasma irradiation for photoinduced decolorization of methylene blue, e-J. Surf. Sci. Nanotech., 12 (2014) 343–348.

TABLE I: Summary of the XPS analysis for V1-V4 samples.

	V1 pristine	V2 oxid. (pristine)	V3 fuzz	V4 oxid. (fuzz)
$V^{4+}p_{3/2}$ [%]	2.4	5.5	9.2	8.8
$V^{5+}p_{3/2}$ [%]	55.3	47.5	42.5	42.4
$V^{5+}p_{1/2}$ [%]	18.7	21.1	21.7	21.9
$V^{5+}p$ [%]	74.0	68.6	64.2	64.3

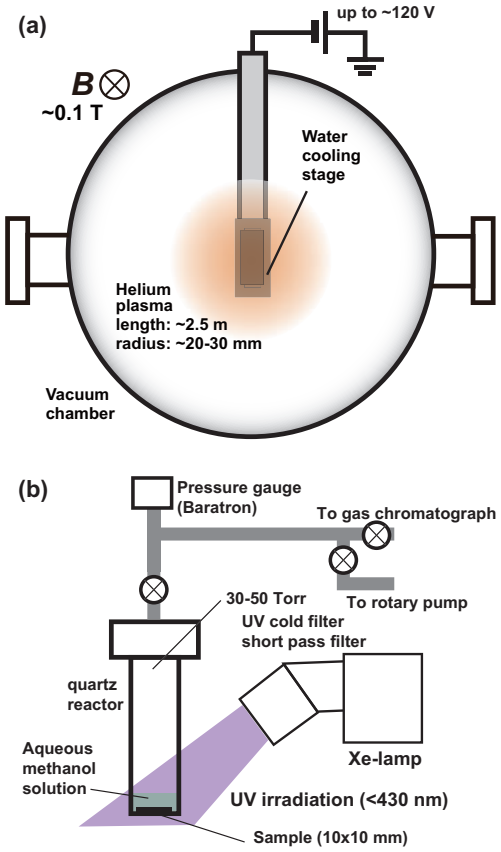

FIG. 1: Schematics of the experimental setup for (a) He plasma irradiation in the linear plasma device NAGDIS-II and (b) photocatalytic H_2 production experiments.

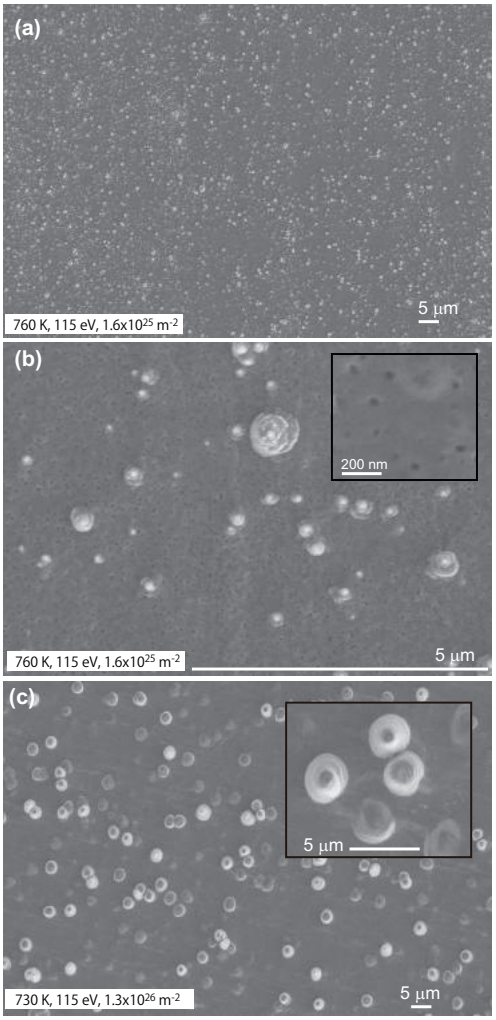

FIG. 2: SEM micrographs of He plasma irradiated vanadium samples. The surface temperature, the incident ion energy, and the He fluence were, respectively, (a,b) 760 K, 115 eV, and 1.6×10^{25} m^{-2} and (c) 730 K, 115 eV, and 1.3×10^{26} m^{-2}.

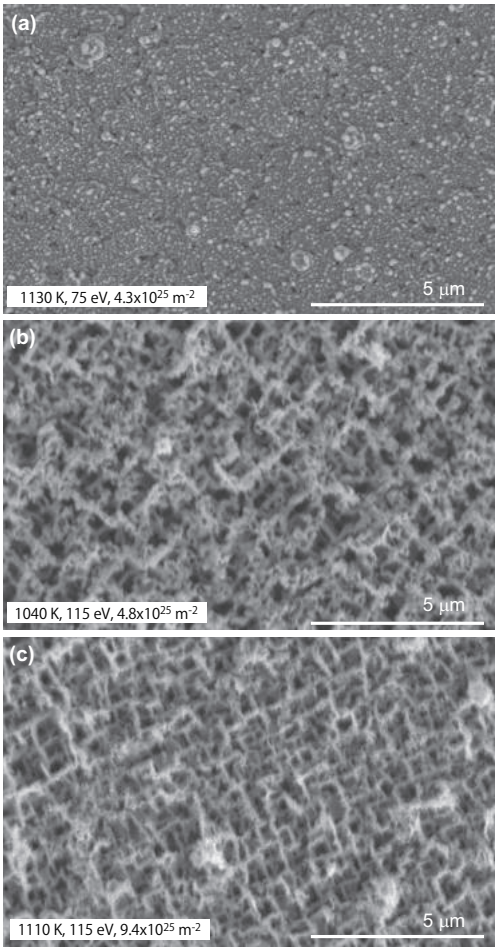

FIG. 3: SEM micrographs of He plasma irradiated vanadium samples. The temperature, the incident ion energy and the He fluence were, respectively, (a) 1130 K, 75 eV, and $4.3\times\ 10^{25}$ m^{-2}; (b) 1040 K, 115 eV, and 4.8×10^{25} m^{-2}; and (c) 1110 K, 115 eV, and 9.4×10^{25} m^{-2}.

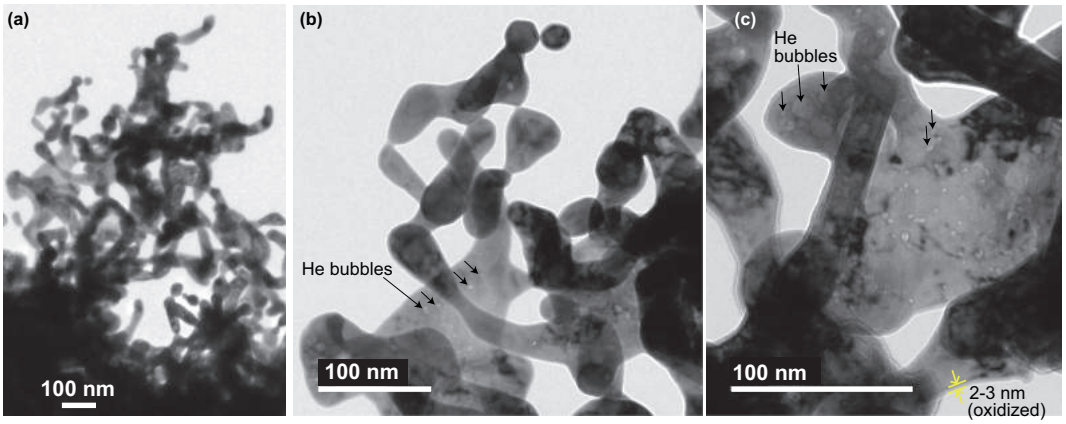

FIG. 4: TEM micrographs of nanostructured V.

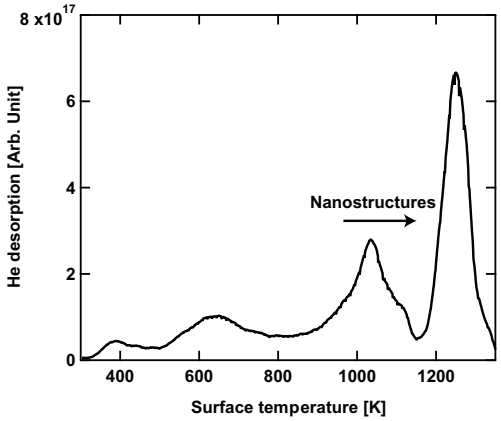

FIG. 5: Thermal desorption spectroscopy spectrum from a He irradiated vanadium sample at 843 K.

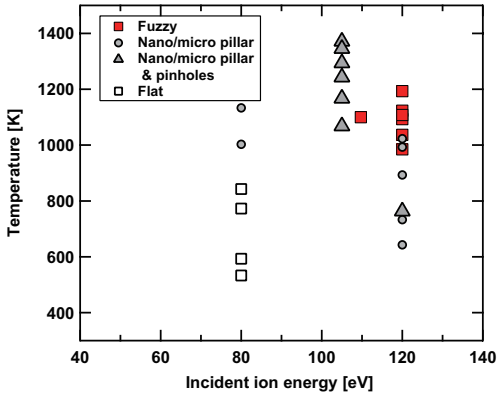

FIG. 6: The relation between the irradiation conditions (the incident ion energy and the surface temperature) and surface morphology changes.

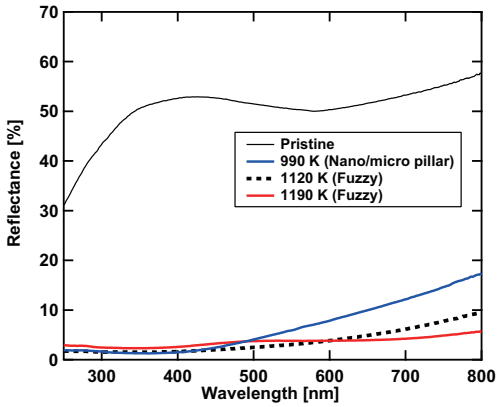

FIG. 7: The wavelength dependence of the optical reflectance of a pristine V sample and the V sample exposed to the He plasmas at 990, 1120, and 1190 K.

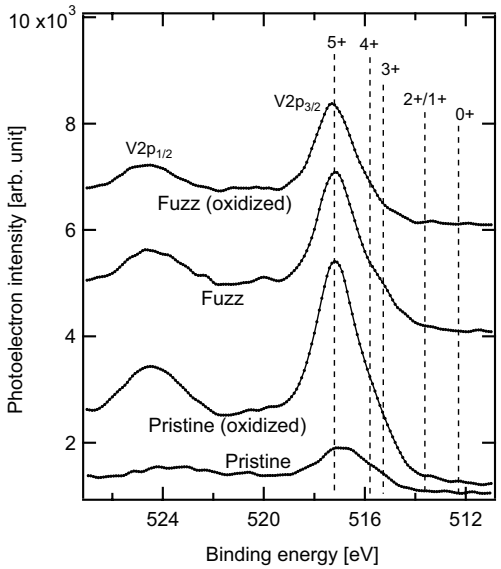

FIG. 8: V2p XPS spectra of the four V samples.

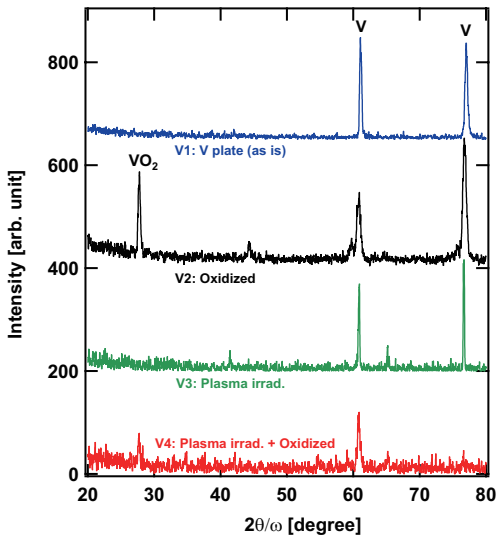

FIG. 9: XRD patterns of the four V samples.

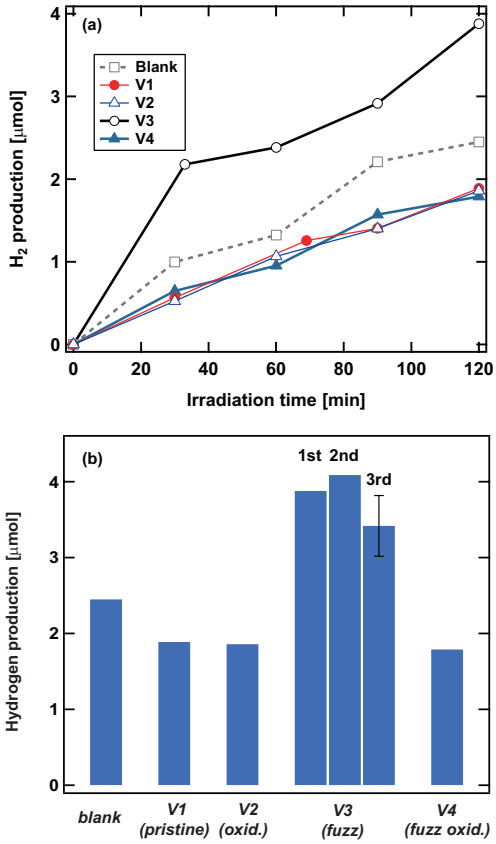

FIG. 10: (a) Time course of produced H_2 from 20 vol.% aqueous methanol solution during UV light irradiation and (b) the total amount of produced hydrogen for 2 hour irradiation.